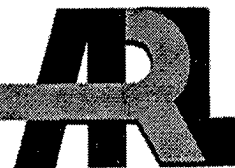


ARMY RESEARCH LABORATORY



Transient Electromagnetic Fields Produced by Pulsed Moving Conductors

by Ira Kohlberg, Alexander Zielinski, and Calvin D. Le

ARL-TR-1931

April 1999

19990419 069

Approved for public release; distribution is unlimited.

DTIC QUALITY INSPECTED 4

The findings in this report are not to be **construed** as an official Department of the **Army** position unless so designated by other authorized documents.

Citation of manufacturer's or trade names does not constitute an official endorsement or approval of **the** use thereof,

Destroy this report when it is no longer needed. Do not return it to the originator.

Army Research Laboratory

Aberdeen Proving Ground, MD 21005-5066

ARL-TR-1931

April 1999

Transient Electromagnetic Fields Produced by Pulsed Moving Conductors

Ira Kohlberg

Kohlberg Associates, Inc.

Alexander E. Zielinski and Calvin D. Le

Weapons and Materials Research Directorate, **ARL**

Abstract

A model was developed for determining the space and time behavior of the magnetic field external to a system of moving pulsed **finite** conductivity conductors. The moving conductor is in relative close proximity to a stationary conductor. The external magnetic field content has a space and time periodicity that is related to the parameters of the system. A numerical example predicts the magnitude and frequency of the magnetic field as a function of distance from the stationary conductor. Potential applications of this study are discussed.

REPORT DOCUMENTATION PAGE			Form Approved OMB No. 0704-0188
Public reporting burden for this collection of information is estimated to average 1 hour per response, including the time for reviewing instructions, searching existing data sources, gathering and maintaining the data needed, and completing and reviewing the collection of information. Send comments regarding this burden estimate or any other aspect of this collection of information, including suggestions for reducing this burden, to Washington Headquarters Services, Directorate for Information Operations and Reports, 1215 Jefferson Davis Highway, Suite 1204, Arlington, VA 22202-4302, and to the Office of Management and Budget, Paperwork Reduction Project (0704-0188), Washington, DC 20503.			
1. AGENCY USE ONLY (Leave blank)	2. REPORT DATE April 1999	3. REPORT TYPE AND DATES COVERED Final, Aug 97 - Oct 98	
4. TITLE AND SUBTITLE Transient Electromagnetic Fields Produced by Pulsed Moving Conductors		5. FUNDING NUMBERS 1L1622618.H80	
6. AUTHOR(S) Ira Kohlberg,* Alexander E. Zielinski, and Calvin D. Le			
7. PERFORMING ORGANIZATION NAME(S) AND ADDRESS(ES) U.S. Army Research Laboratory ATTN: AMSRL-WM-BC Aberdeen Proving Ground, MD 21005-5066		8. PERFORMING ORGANIZATION REPORT NUMBER ARL-TR-1931	
9. SPONSORING/MONITORING AGENCY NAMES(S) AND ADDRESS(ES)		10. SPONSORING/MONITORING AGENCY REPORT NUMBER	
11. SUPPLEMENTARY NOTES *Kohlberg Associates, Inc., 11308 South Shore Road, Reston, VA 20190			
12a. DISTRIBUTION/AVAILABILITY STATEMENT Approved for public release; distribution is unlimited.		12b. DISTRIBUTION CODE	
13. ABSTRACT (Maximum 200 words) A model was developed for determining the space and time behavior of the magnetic field external to a system of moving pulsed finite conductivity conductors. The moving conductor is in relative close proximity to a stationary conductor. The external magnetic field content has a space and time periodicity that is related to the parameters of the system. A numerical example predicts the magnitude and frequency of the magnetic field as a function of distance from the stationary conductor. Potential applications of this study are discussed.			
14. SUBJECT TERMS magnetic field, environment		15. NUMBER OF PAGES 58	
		16. PRICE CODE	
17. SECURITY CLASSIFICATION OF REPORT UNCLASSIFIED	18. SECURITY CLASSIFICATION OF THIS PAGE UNCLASSIFIED	19. SECURITY CLASSIFICATION OF ABSTRACT UNCLASSIFIED	20. LIMITATION OF ABSTRACT UL

INTENTIONALLY LEFT BLANK

Acknowledgments

The authors wish to thank Mrs. Sharon Y. Wiley for her assistance in typing this manuscript and in developing the illustrations. Also, a sincere appreciation is extended to Mr. John Bennett, U.S. Army Armaments Research, Development, and Engineering Center (ARDEC) for a concise and thorough review.

INTENTIONALLY LEFT BLANK

Table of Contents

	<u>Page</u>
Report Documentation Page	iii
Acknowledgments.....	v
List of Figures	ix
1. Introduction	1
2. Theoretical Considerations.....	4
3. Electromagnetic Fields and Currents in a Moving Conductor.....	16
4. Characterization of External Magnetic Field	27
5. Numerical Results	44
6. Summary and Conclusion	47
7. References	49
Distribution List	51

INTENTIONALLY LEFT BLANK

List of Figures

<u>Figure</u>	<u>Page</u>
1. Source Current Elements and Moving Conductor	2
2. Geometric Considerations for Determining the Environmental Magnetic Field Produced by a Moving Conductor System.....	3
3. Single Source Current Element and Its Image for an Infinite Conductive Surface	5
4. Approximate Image Theory for Conducting Ground Plane	13
5. $h_n^2(t)$ as a Function of Time With Mode Index, n , as Parameter	36
6. $H_n^2(t)$ as a Function of Time With Mode Index, n , as Parameter	36
7. $P_n(\eta)$ as a Function of Positive η With Mode Index, n , as Parameter	43
8. Magnetic Field as a Function of Dimensionless Distance	46

INTENTIONALLY LEFT BLANK

1. Introduction

Over the years, there has been continuing interest in the development of pulsed-power energy sources and accelerators based on the processes of transient magnetic field exclusion and diffusion. An essential feature of these devices involves a stationary source current and the generation of induced currents (i.e., eddy currents) in a moving finite conductivity conductor. The source and eddy currents produce magnetic fields external to their geometry that have a characteristic magnitude and frequency. Applications utilizing this process can be found in electromagnetic braking of large electromechanical systems [1, 2, 3] and the generation of high electrical power pulses [4, 5]. These applications require *100's* of *kA* with millisecond pulse-widths. Additionally, these currents can produce external magnetic fields of a few Tesla.

As these electrical devices mature into components for military systems, we must consider the electromagnetic compatibility (EMC) issues that arise from the “environmental” electric and magnetic fields they generate. By “environmental” fields, we mean those fields that are created in spatial locations that are not especially close to the regions that they originate from and are concurrently located in close proximity to electronic equipment that may be affected by them. For example, we have found that environmental electromagnetic fields generated by capacitor-driven pulsed-power sources could be important EMC considerations for electromagnetic railguns [6, 7]. Fortunately, standard shielding techniques, using conducting materials, are adequate for managing all but the largest magnetic fields (i.e., $< 1T$) [8]. For large confined fields, active shielding techniques can be more efficiently implemented [8].

The purpose of this initial assessment is to characterize the salient features of the environmental magnetic field generated by a moving conductor system that is produced by a spatially periodic time-varying source current. Figure 1 shows a close-up of the relationship between the spatially periodic source currents and the moving conductor.

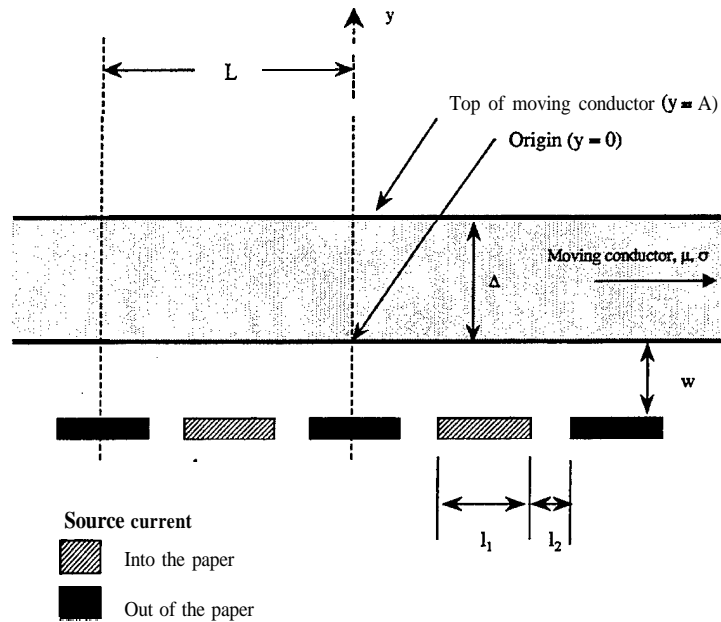


Figure 1. Source Current Elements and Moving Conductor.

Figure 2 shows the geometry used for determining the environmental magnetic field. The object of this study is to determine the time behavior of the magnetic field at point $P(x_o, y_o, z_o)$ due to the source currents. In Figure 2, the system is assumed to be periodic and infinite in the $\pm x$ -directions. We have cast the problem in Cartesian coordinates for mathematical simplicity, but, with the proper mathematical transformation, it can be made to correspond to cylindrical geometry.

In this report, no attempt is made to relate the test results to a specific application. A significant amount of detailed information would be required to accomplish this, and such an effort is beyond the scope of the present study.

The results of our model quantify the damped harmonic electromagnetic fields generated by a moving conductor in terms of the periodic spatial separation between the current sources, the conductivity and velocity of the moving conductor, and the location of the observation point relative to the moving conductor. The principal contributions to the far-field magnetic signature, however, are shown to be due to the source current distribution and its time-dependent image created during a transient pulse.

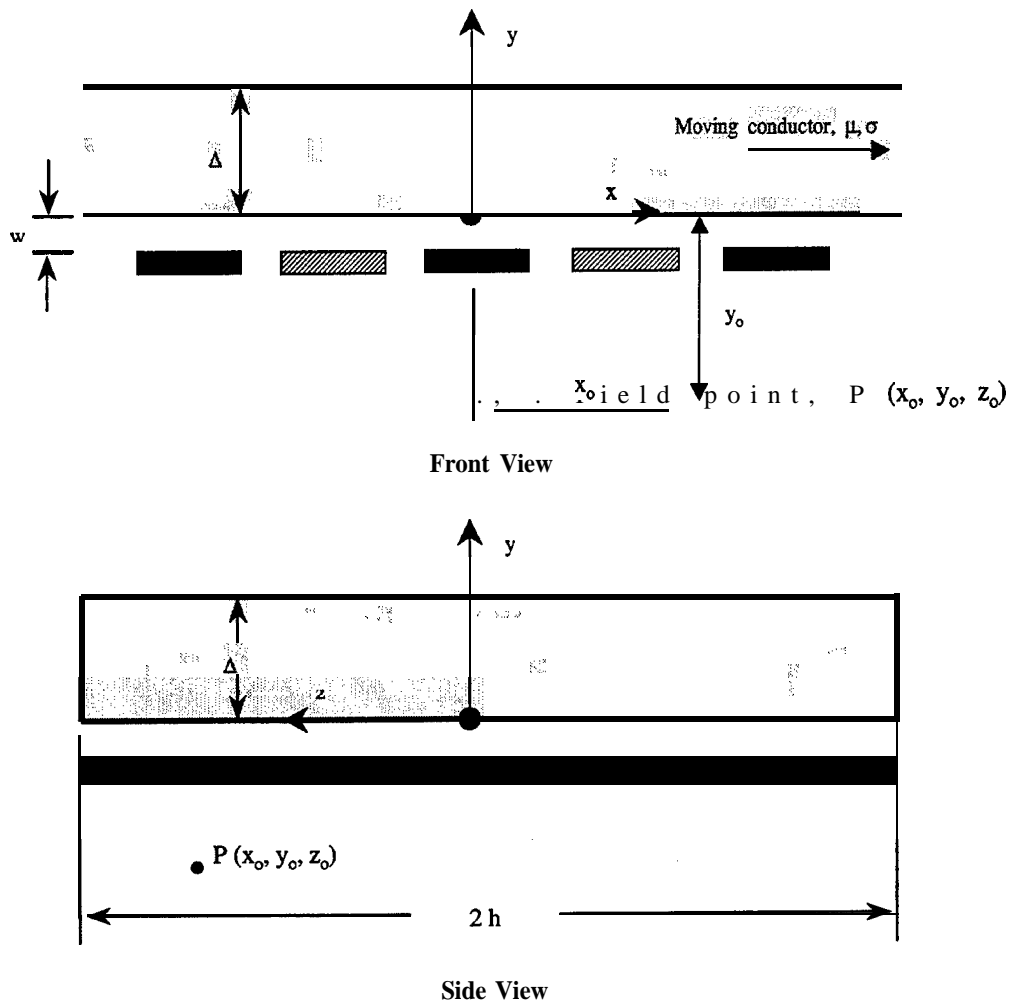


Figure 2. Geometric Considerations for Determining the Environmental Magnetic Field Produced by a Moving Conductor System.

The mathematical details leading to the determination of the current density in the moving conductor and the subsequent prediction of the environmental magnetic field are tedious to follow. In order to facilitate the process of understanding the basic physical ideas, analysis, and interpretation of the results, a brief overview of the basic physical processes is presented in section 2. The theoretical prediction of the current density and associated magnetic fields in the moving conductor is rendered in section 3. Using the results of section 3, the environmental magnetic field is computed in section 4. Numerical results are rendered in section 5. Summary and conclusions are presented in section 6.

2. Theoretical Considerations

Much insight into the structure of the electromagnetic fields described in Figures 1 and 2 can be gleaned by first considering the solution for a single-source current element. For convenience, we select the center source element of Figures 1 and 2. Elucidation of the essential physical phenomena is further facilitated by considering the two-dimensional case in which source current elements are infinite in the z -direction and where the thickness, A , is suitably large. The implications of this latter assumption are defined in the course of the discussion.

For illustration, we begin with the case in which the conductor's velocity is zero. We want to determine the response of this nonmoving conductor to a sudden increase in the source current, $I(t) : t \geq 0$, which flows through each source element. (The origin of $I(t)$ is not essential for understanding the issues related to the electromagnetic fields. Nevertheless, it is worthwhile to mention that, in the case of an energy-producing device, $I(t)$ is determined from external considerations that involve: generation of an electromotive force in the stationary conductor, an electrical load, and the current induced in the moving conductor by $I(t)$ itself. For example, in the case of a compensated pulsed alternator [5], the effect of the moving conductor is to produce a time-dependent mutual inductance. Detailed discussions on the types of compensation and the methods for the physical realization of compensation in pulsed machinery can be found in the literature [5].)

The problem of the stationary conductor further divides into two categories: (1) the case where the conductivity of the moving conductor is infinite and (2) the case where the conductivity is finite. A close-up of the situation for a single conductor with $\sigma = \infty$ is shown in Figure 3.

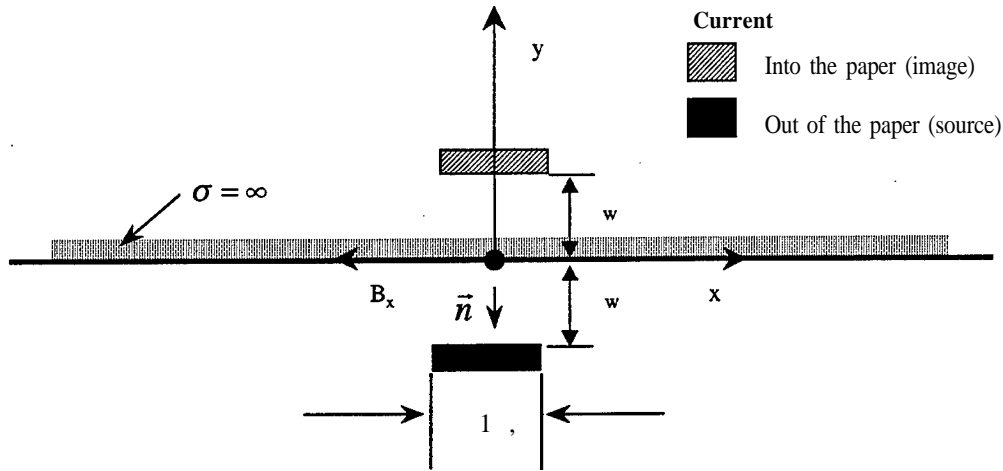


Figure 3. Single Source Current Element and Its Image for an Infinite Conductive Surface.

The basic physical law that determines the current flow in the case where $\sigma = \infty$ is concerned not with the magnetic field, but with the electric field. The surface impedance for a medium that has infinite conductivity is identically zero. This requires that the total component of the electric field on the surface, which is parallel to the surface, \mathbf{E}_{\parallel} , must also be identically zero. A reflected electromagnetic wave must therefore have its component of the surface electric field that is parallel to the surface exactly cancel the corresponding component of the incident electric field [9]. The only component of the electric field that can exist on the surface of a perfect conductor is the component that is normal to the surface, \mathbf{E}_{\perp} .

The foregoing discussion concerning \mathbf{E}_{\parallel} applies at all frequencies. It can be shown using the theory of a horizontal dipole over a conducting half space, taken in the limit of $\sigma = \infty$, that the condition $\mathbf{E}_{\parallel} = 0$ leads to image theory [9]. When applied to Figure 3, image theory shows that the magnetic field at the surface of an infinite conducting body can be computed from two sources [9]. The first source is the true physical current source (flowing out of the paper), and the other is the image of the source current that flows into the paper.

Image theory permits the field at all points in space to be computed by summing the fields due to the actual physical real source and its image. The real source and its image each produce a magnetic field determined from the Biot-Savart law [9]. The three dimensional form of the Biot-Savart is given by

$$\vec{B} = \frac{\mu_0}{4\pi} \iiint \frac{\vec{j}_c(\bar{x}, \bar{y}, \bar{z}) \times \vec{r}}{|\vec{r}|^3} d\bar{x}d\bar{y}d\bar{z}, \quad (1)$$

where \vec{j}_c is the current density; $\bar{x}, \bar{y}, \bar{z}$ are the coordinates of the volumetric distribution of \vec{j}_c ; and x, y, z are the coordinates at which the field is to be computed;

$$\vec{r} = \vec{i}(x - \bar{x}) + \vec{j}(y - \bar{y}) + \vec{k}(z - \bar{z}) \quad (2)$$

and

$$|\vec{r}|^3 = ((x - \bar{x})^2 + (y - \bar{y})^2 + (z - \bar{z})^2)^{3/2}, \quad (3)$$

where \vec{i}, \vec{j} , and \vec{k} are unit vectors in the x -, y -, and z -directions, respectively. For currents that flow only in the z -direction, we have

$$\vec{j}_c = j_c(\bar{x}, \bar{y}, \bar{z})\vec{k} \quad (4)$$

and

$$\vec{k} \times \vec{r} = \vec{j}(x - \bar{x}) - \vec{i}(y - \bar{y}). \quad (5)$$

When applied to the two-dimensional configuration of Figure 3, the contributions from the real source, \vec{B}_R , and image, \vec{B}_I , are given by

$$\vec{B}_R = \frac{\mu_o}{4\pi} J_o(t) \int_{-l_1/2}^{+l_1/2} \int_{-\infty}^{+\infty} \frac{\vec{j}(x-\bar{x}) - \vec{i}(y+w)}{\left((x-\bar{x})^2 + (y+w)^2 + (z-\bar{z})^2\right)^{3/2}} d\bar{z} d\bar{x} \quad (6)$$

and

$$\vec{B}_I = -\frac{\mu_o}{4\pi} J_o(t) \int_{-l_1/2}^{+l_1/2} \int_{-\infty}^{+\infty} \frac{\vec{j}(x-\bar{x}) - \vec{i}(y-w)}{\left((x-\bar{x})^2 + (y-w)^2 + (z-\bar{z})^2\right)^{3/2}} d\bar{z} d\bar{x}, \quad (7)$$

where

$$J_o(t) = \frac{I(t)}{l_1} \quad (8)$$

is the current per unit length of the source current element. When equations (6) and (7) are evaluated on the surface of the conductor, $y = 0$, we find that the y-component of the magnetic field vanishes and the x-component, B_{sx} , consists of equal contributions from the real source and its image. We get

$$B_{sx}(x) = -\frac{\mu_o}{2\pi} J_o(t) w \int_{-l_1/2}^{+l_1/2} \int_{-\infty}^{+\infty} \frac{1}{\left((x-\bar{x})^2 + (w)^2 + (z-\bar{z})^2\right)^{3/2}} d\bar{z} d\bar{x}. \quad (9)$$

Integration over \bar{z} gives

$$B_{sx}(x) = -\frac{\mu_o}{\pi} J_o(t) w \int_{-l_1/2}^{+l_1/2} \frac{d\bar{x}}{(x-\bar{x})^2 + w^2} = B_{sx}(-x). \quad (10)$$

Using the principle of superposition, the total surface magnetic field corresponding to the alternating array of Figure 1 is

$$B_{sx}^T = \sum_{n=-\infty}^{n=+\infty} B_{sx} \left(x - \frac{nL}{2}\right) (-1)^n. \quad (11)$$

By making the substitution $x = x + mL$, where m is any integer, in equation (11), we easily see that B_{sx}^T is a periodic function of L . We derive

$$B_{sx}^T(x + mL) = \sum_{n'=-\infty}^{n'=+\infty} B_{sx} \left(x - \frac{n'L}{2}\right) (-1)^{n'}, \quad (12)$$

where the new dummy variable of summation is now $n' = 2m - n$. Since n and n' are summation indices, equation (11) is the same as equation (12).

Combining the symmetry and periodic properties of B_{sx}^T , we can write

$$B_{sx}^T = \sum_{n=1}^{n=\infty} B_{sx}^n(t) \cos \frac{2n\pi x}{L}, \quad (13)$$

where

$$B_{sx}^n = \frac{2}{L} \int_0^L \cos \frac{2n\pi x}{L} B_{sx}^T dx. \quad (14)$$

The modal components, B_{sx}^n , are determined by straightforward integration of equation (14) using equations (10) and (11). The details of the calculation are not important. It is important to note, however, that all B_{sx}^n are proportional to the product of $-\mu_o J_o(t)$. Accordingly, it is convenient to use the form

$$B_{sx}^n = -\mu_o J_o(t) \Omega_n, \quad (15)$$

where the Ω_n are shown to be dimensionless expansion coefficients given by

$$\Omega_n = \frac{2}{L} \int_0^L \cos \frac{2n\pi x}{L} \left[\sum_{n'=-\infty}^{n'+\infty} (-1)^{n'} \frac{w^{+i/2}}{\pi^{-i/2}} \int \frac{d\bar{x}}{(x - \frac{n'L}{2} - \bar{x})^2 + w^2} \right] dx. \quad (16)$$

The magnetic field intensity at the surface due to all the conductors is

$$H_{sx}^T = \frac{B_{sx}^T}{\mu_o} = -J_o(t) \sum_{n=1}^{\infty} \Omega_n \cos \frac{2n\pi x}{L}. \quad (17)$$

The general expression for the surface current density, \vec{J}_s , is given by the vector equation

$$\vec{n} \times \vec{H}_s = \vec{J}_s, \quad (18)$$

where \vec{H}_s is magnetic field intensity on the surface and \vec{n} is the normal to the surface of the conductor. As shown in Figure 3, \vec{n} points in the negative y-direction and

$$\vec{H}_s = \vec{i} H_{sx}^T = -\vec{i} J_o(t) \sum_{n=1}^{\infty} \Omega_n \cos \frac{2n\pi x}{L}. \quad (19)$$

Inserting equation (19) into (18) gives

$$\vec{J}_s = -\vec{k} J_o(t) \sum_{n=1}^{\infty} \Omega_n \cos \frac{2n\pi x}{L}. \quad (20)$$

In contrast to the discontinuous elements of the array shown in Figure 1, the current density on the surface is always continuous because the surface is continuous. For example, in the case of a single element, which is discontinuous, the surface magnetic field has been shown in equation (10) to be continuous. Using equation (10) in

equation (18) then provides a continuous surface current. Discontinuities in surface current lead to singular point accretions of charge on the surface. This does not appear to be physically plausible in this problem.

Equation (20) shows that \vec{J}_s is a periodic function of x . By comparison, the discontinuous current density, \vec{J}_R , of the periodic distribution of source elements shown in Figures 1 and 2 can be written as $\vec{J}_R = \vec{k}J_R$. The magnitude is

$$J_R(x,t) = \sum_{n=0}^{\infty} A_n(t) \cos \frac{2n\pi x}{L}, \quad (21)$$

where

$$L = 2(l_1 + l_2), \quad (22)$$

and the A_n 's are determined from the orthogonality properties of the Fourier series. Using the discontinuous distributions

$$J(x,t) = J_o(t) \quad : \frac{l_1}{2} \geq |x| \geq 0,$$

$$= 0 \quad : \frac{l_1}{2} + l_2 \geq |x| \geq \frac{l_1}{2},$$

and

$$= -J_o(t):l_1 + l_2 \geq |x| \geq \frac{l_1}{2} + l_2, \quad (23)$$

we derive

$$A_n = \frac{2J_o(t)}{n\pi} (1 - \cos n\pi) \sin \frac{n\pi l_1}{L}. \quad (24)$$

The image distribution for the array of source elements is the negative of equation (21).

In contrast to the image current, which is a mathematical abstraction, the surface current of equation (20) is a real current. However, from the point of view of calculating the conductor's contribution to the magnetic field for $y < 0$ from the Biot-Savart law, we have a choice of using either the real surface current located at $y = 0$ or the image current located in the plane $y = w$.

In summary, we have learned the following from the infinite conductivity case that has bearing on the general case involving a moving conductor having finite conductivity.

- (1) A true physical surface current is produced on the conductor that is generated by the source current array.
- (2) The physical surface current is computed from the source current and its image.
- (3) The surface current is continuous.
- (4) The time behavior of the surface current and its image is proportional to the time behavior of the source current. For example, if the source current were to remain

constant in time, so would the surface current and the image current. The reason for this is that infinite conductivity precludes energy dissipation and, hence, a current once generated will persist indefinitely (in the absence of radiation losses).

We now consider a nonmoving conductor with finite conductivity. This extension is one that involves an enormous increase in complexity as compared with the infinite conductivity case. As previously mentioned, the basic physical problem to be solved here is that of a horizontal dipole over a conducting ground plane. This problem was first attacked by the German theoretical physicist, Arnold Sommerfeld, at the beginning of the 20th century, and, for the first half of this century, played a crucial role in the field of radio science. Analytic study of the famous “Sommerfeld Integrals” connected with the solution continues to this very day. The seminal text by Banos [10] provides a comprehensive discussion of this fundamental and difficult problem.

The solution for the horizontal dipole over a conducting ground furnishes a complete space-and-time description of the electric and magnetic fields both inside the conductor and in free space. For example, Hill and Wait [11] solve explicitly for the fields in the case where the line source lies directly on the ground. Our problem is simply an extension of the basic problem to include a finite number of distributed elements. Although this type of rigorous formulation can be attempted, it is not worthwhile to do so unless we can demonstrate that simpler models can't do the job.

The literature on horizontal dipoles over ground planes is extensive and has been addressed by the leading electromagnetic theoreticians in this century. A major outcome of these studies has been the emergence of an approximate image theory that is applicable for conducting media [12]. Figure 4 shows how this theory is applied. If w is the location of the image for $\sigma = \infty$, the total displacement, w_c , for $\sigma \neq \infty$ is given by [12]

$$w_c = w + d, \tag{25}$$

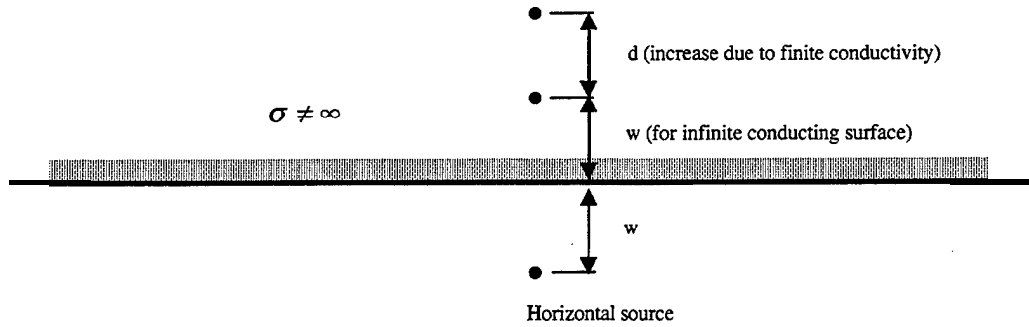


Figure 4. Approximate Image Theory for Conducting Ground Plane.

where d is the additional displacement due to the conductivity. In frequency space, d is actually a complex quantity, a consequence of fitting the rigorous theory with a mathematical approximation [12]. It is given by

$$d = \frac{2}{(j\omega \mu_0 \sigma)^{1/2}}, \quad (26)$$

which is valid for the condition, $\sigma \gg \omega \epsilon$ (applicable in our case).

If we associate the magnitude of d with the physical displacement and let $\omega \approx 2\pi / t_p$, where t_p is the duration of a pulse, we obtain

$$|d| = \sqrt{\frac{2t_p}{\pi \mu_0 \sigma}}. \quad (27)$$

Equation (27) is (within a numerical constant of order unity) the root-mean-square displacement determined from diffusion theory. If t_p is small, the displacement of the image will likewise be small. Equation (27) thus provides the physically intuitive result that, for short times, the location of the image is that obtained from the $\sigma = \infty$ case. In

order to apply equation (27) with any degree of confidence, the thickness, A , must be greater than $|d|$.

In order to use image theory, we need to know not only its displacement, but also the magnitude of the image current. Whereas in the $\sigma = \infty$ case, the magnitude of the image current is equal to that of the source current, this will not rigorously be true in the finite conductivity case. The magnitude of the image current will be less than that for the infinite conducting case because there are energy losses in the system associated with finite conductivity. The rigorous solution of this problem requires the formulation in terms of a frequency-dependent horizontal dipole over a conducting half space [10].

When the velocity is not zero, the location of the image is the same as that for the stationary conductor for $\sigma = \infty$. The reason for this is the same as before: the only way we can assure zero electric field at the surface is for the image to be opposite to the real source. Since the source is stationary, so is the image.

An explanation of current behavior when the conductor is moving and $\sigma \neq \infty$ is not easily explained without solving the entire problem. Conceptually, this problem can be attacked as a moving horizontal dipole over a conducting half space. To our knowledge, this approach has not been attempted. By all reckoning, it would appear to be an extremely difficult problem. Nevertheless, this is the problem that is addressed in this study.

Our solution is based on solving Maxwell's equations,

$$\nabla \times \vec{H} = \sigma \vec{E} + \sigma \vec{V} \times \vec{B} , \quad (28a)$$

$$\nabla \times \vec{E} = -\frac{\partial \vec{B}}{\partial t} , \quad (28b)$$

$$\vec{B} = \mu_0 \vec{H}, \quad (28c)$$

and

$$\nabla \cdot \vec{B} = 0 \quad (28d)$$

in a conductor moving with velocity, V . In our model, it is assumed that the conductor's thickness, A , is large enough so that the electromagnetic fields never diffuse out of the moving conductor. Mathematically, the large enough assumption means that we can set the magnetic field components equal to zero at $y = A$.

The foregoing assumption about A being large has only an indirect bearing on the calculation of the environmental magnetic field **from** the currents in the system. What is really important is the depth of penetration of the current into the moving conductor as compared with the vertical distance of the field point at which the magnetic field is being calculated from the conductor surface. As we show in this study, the depth of magnetic field penetration is quite small compared with meaningful distances.

An accurate prediction of the fields is possible, provided that we can precisely specify the magnetic field at the bottom surface for all time, $t \geq 0$. This is exactly where the difficulty arises; the magnetic field at $y = 0$ cannot precisely be defined for all time without simultaneously solving Maxwell's equations in the space below the moving conductor.

It would appear that an approximate solution to this problem can be obtained using perturbation theory. The concept is as follows: first, we solve for the electromagnetic fields in the conductor by assuming that the magnetic field at $y = 0$ is given by image theory for $\sigma = \infty$. This approximation enables us to determine the first-order correction for the displacement of the image due to diffusion and the decrease in the magnitude of

the image current due to energy losses associated with finite conductivity. Corrections to the surface magnetic field are then made.

3. Electromagnetic Fields and Currents in a Moving Conductor

Maxwell's equations in a moving conductor are given by equation (28). In the geometry of Figures 1 and 2, the velocity is given by the relationship: $\vec{V} = \vec{i}v$. By taking the curl of equation (28a) and making the substitutions of equations (28b) and (28c) for $\nabla \times \vec{E}$ and \vec{H} in equation (28a), we derive the following identical equations for B_x and B_y :

$$\frac{1}{\mu\sigma} \left[\frac{\partial^2 B_x}{\partial x^2} + \frac{\partial^2 B_x}{\partial y^2} \right] = \frac{\partial B_x}{\partial t} + v \frac{\partial B_x}{\partial x}, \quad (29a)$$

and

$$\frac{1}{\mu\sigma} \left[\frac{\partial^2 B_y}{\partial x^2} + \frac{\partial^2 B_y}{\partial y^2} \right] = \frac{\partial B_y}{\partial t} + v \frac{\partial B_y}{\partial x}. \quad (29b)$$

Equations (29a - b) are, however, not entirely independent. The divergence condition of equation (28d),

$$\nabla \cdot \vec{B} = 0 = \frac{\partial B_x}{\partial x} + \frac{\partial B_y}{\partial y} = 0, \quad (30)$$

creates an interdependency on the solutions of equations (29a - b). They are each second-order in x and y , and first-order in time. If it were not for the divergence relationship, they would be completely independent. For the boundary conditions of our problem, we

readily show that the solution of equation (29a) combined with equation (30) uniquely determines B_y .

Let us first consider the solution for B_x . We must specify the boundary conditions at $y=0$ and at $y= A$. The boundary condition at $y = A$ is greatly simplified for pulse lengths, t_p , that are short (i.e., $A \gg d$). When these conditions apply, we are at liberty to set both components of the magnetic field equal to zero at the top boundary:

$$B_x(x, y = A, t) = B_y(x, y = A, t) = 0. \quad (31)$$

This is the boundary condition used in our study.

The foregoing boundary will be relevant only for those cases where the diffusion time, t_D , from the initiation of the pulse at $y = 0$ to $y = A$ is larger than t_p . The diffusion time is approximated by the formula

$$t_D \approx \Delta^2 \mu_0 \sigma. \quad (32)$$

Diffusion time can vary greatly, depending on the application. For example, using an aluminum conductor ($\sigma = 2.2 \times 10^7$ mhos/m, $\mu_0 = 4\pi \times 10^{-7}$ H/m), and a nominal thickness $A = 1.5$ cm gives

$$t_D = 6.2 \text{ ms}. \quad (33)$$

When t_p is significantly shorter than t_D , the top boundary of Figure 1 is never reached during its duration and, for all practical purpose, it could be located at $y = \infty$. On the other hand, for a system in which there is a continuous stream of pulses, the condition at the top boundary may need to be more critically examined.

The solution of the problem requires that we specify the time behavior for B_x at $y=0$ for $t \geq 0$. This quantity is denoted in this section as

$$B_x^o = B_x(x, y = 0, t). \quad (34)$$

B_x^o is determined from the considerations rendered in section 2. For example, we can set

$$B_x^o = -\mu_o J_o(t) \sum_{n=1}^{n=\infty} \Omega_n \cos \frac{2n\pi x}{L}, \quad (35)$$

which is the field due to the periodic source of Figure 1 over a perfectly conducting plane. Use of equation (35) constitutes the **first** approximation in a perturbation scheme.

Our analysis, however, 'is carried out in general terms by keeping the spatial periodicity and allowing for an arbitrary time behavior in $J_o(t)$. This is accomplished using a Delta (impulse) function current density source. The boundary condition at $y = 0$ then becomes

$$B_x^o = -\mu_o \delta(t) \sum_{n=1}^{n=\infty} \Omega_n \cos t. \quad (36)$$

If B_x and B_y **are** now interpreted as the solutions to equations (29a) and (29b) for the impulse function, the actual fields, $B_x^A(x, y, t)$ and $B_y^A(x, y, t)$ will be given by

$$B_x^A(x, y, t) = \int_0^t B_x(x, y, \tau) J_o(t - \tau) d\tau, \quad (37a)$$

and

$$B_y^A(x, y, t) = \int_0^t B_y(x, y, \tau) J_o(t - \tau) d\tau. \quad (37b)$$

In section 4, we apply the foregoing formulas to the case where $J_o(t)$ is a step function that has the properties

$$J_o = A_J \quad : t_p \geq t \geq 0 \quad (38a)$$

$$J_o = 0 \quad : t \geq t_p, \quad (38b)$$

where A_J is a constant.

Denoting the **Laplace** transform variable by “s” gives

$$\frac{1}{\mu_o \sigma} \left[\frac{\partial^2 \tilde{B}_x}{\partial x^2} + \frac{\partial^2 \tilde{B}_x}{\partial y^2} \right] = s \tilde{B}_x + v \frac{\partial \tilde{B}_x}{\partial x}, \quad (39)$$

where \tilde{B}_x is defined as the **Laplace** transform of B_x . The foregoing equation is next reduced to one involving only the y-dimension by using the periodicity of the x-direction. We have

$$\tilde{B}_x(x + L, y, s) = \tilde{B}_x(xy, s). \quad (40)$$

Using equation (40), we next write \tilde{B}_x as the real part of the harmonic series

$$\tilde{B}_x = \sum_{n=-\infty}^{n=+\infty} \tilde{f}_n(y, s) e^{i\gamma_n x}, \quad (41)$$

where

$$\gamma_n = \frac{2n\pi}{L}. \quad (42)$$

Substituting equation (41) into equation (39) and equating terms proportional to $e^{j\gamma_n x}$ gives the following differential equation for $\tilde{f}_n(y, s)$:

$$\frac{\partial^2 \tilde{f}_n}{\partial y^2} - (\gamma_n^2 + \mu_o \sigma s + j\mu_o \sigma v \gamma_n) \tilde{f}_n = 0. \quad (43)$$

The solution for \tilde{f}_n is

$$\tilde{f}_n = \tilde{E}_n e^{k_n y} + \tilde{F}_n e^{-k_n y}, \quad (44)$$

where

$$k_n = \sqrt{\gamma_n^2 + \mu_o \sigma s + j\mu_o \sigma v \gamma_n}. \quad (45)$$

Since the magnetic field must go to zero at $y = \infty$, we require that $\tilde{E}_n = 0$ and thus have

$$\tilde{f}_n = \tilde{F}_n e^{-k_n y}. \quad (46)$$

Inserting equation (46) into equation (41) gives

$$\tilde{B}_x = \sum_{n=-\infty}^{n=+\infty} \tilde{F}_n(s) e^{-k_n y} e^{j\gamma_n x}. \quad (47)$$

Using the same methodology for equation (29b), we derive the following expression for B_x :

$$\tilde{B}_y = \sum_{n=-\infty}^{n=+\infty} \tilde{P}_n(s) e^{-k_n y} e^{j\gamma_n x}, \quad (48)$$

where $\tilde{P}_n(s)$ is related to $\tilde{F}_n(s)$ through the divergence relationship of equation (30):

$$\frac{\partial \tilde{B}_x}{\partial x} + \frac{\partial \tilde{B}_y}{\partial y} = \sum_{n=-\infty}^{n=+\infty} (j\gamma_n \tilde{F}_n(s) - k_n \tilde{P}_n) e^{-k_n y} e^{j\gamma_n x} = 0. \quad (49)$$

The only way that equation (49) can be satisfied is if the “()” terms are equal to zero.

Setting these terms equal to zero gives

$$\tilde{P}_n = \frac{j\gamma_n}{k_n} \tilde{F}_n(s). \quad (50)$$

From the foregoing equations, we see that the \tilde{F}_n ‘s determine the x- and y-components of the electromagnetic field. The \tilde{F}_n ‘s are determined from the boundary condition of equation (36) applied in **Laplace** transform space. Recalling that

$$\tilde{\mathcal{L}} \delta(t) = 1, \quad (51)$$

where $\tilde{\mathcal{L}}$ is the **Laplace** transform operator, and evaluating equation (47) at $y = 0$ gives

$$\tilde{B}_x^o = -\mu_o \sum_{n=1}^{\infty} \Omega_n \cos \frac{2n\pi x}{L} = \sum_{n=-\infty}^{n=+\infty} \tilde{F}_n(s) e^{j\gamma_n x}. \quad (52)$$

Using $e^{j\gamma_n x} = \cos \gamma_n x + j \sin \gamma_n x$ gives

$$\sum_{n=-\infty}^{n=+\infty} \tilde{F}_n(s) e^{j\gamma_n x} = \tilde{F}_o + \sum_{n=1}^{\infty} [(\tilde{F}_n + \tilde{F}_{-n}) \cos \gamma_n x + j(\tilde{F}_n - \tilde{F}_{-n}) \sin \gamma_n x]. \quad (53)$$

Inserting equation (53) into equation (52) and noting that there is no Ω_0 term in equation (52) gives

$$\tilde{F}_n + \tilde{F}_{-n} = -\mu_o \Omega_n, \quad (54a)$$

$$\tilde{F}_n - \tilde{F}_{-n} = 0, \quad (54b)$$

and

$$\tilde{F}_o = 0. \quad (54c)$$

From equations (54a - c), we have

$$\tilde{F}_n = \tilde{F}_{-n} = \frac{-\mu_o \Omega_n}{2}. \quad (55)$$

The time domain x-component of the magnetic field is obtained by taking the inverse Laplace transform of equation (47):

$$B_x(x, y, t) = \sum_{n=-\infty}^{n=+\infty} \int_0^t F_n(t-\tau) Q_n(\tau) d\tau e^{j\gamma_n x}, \quad (56)$$

where $F_n(t)$ is the inverse Laplace transform of $\tilde{F}_n(s)$ and

$$Q_n(\tau) = \tilde{L}^{-1}(e^{-k_n \tau}) = \tilde{L}^{-1} \tilde{q}_n(s). \quad (57)$$

$Q_n(\tau)$ is computed in two steps. First, we write

$$k_n = \sqrt{\mu_o \sigma} \sqrt{s + r_n}, \quad (58)$$

where

$$r_n = \frac{\gamma_n^2}{\mu_o \sigma} + j\nu\gamma_n. \quad (59)$$

Then

$$\tilde{q}_n(s) = e^{-\left(\sqrt{\mu_o \sigma y^2} \sqrt{s+r_n}\right)}. \quad (60)$$

From the properties of the inverse Laplace transform, we have

$$\tilde{L}^{-1}\tilde{q}_n(s) = e^{-r_n t} \tilde{L}^{-1}\left(e^{-\alpha\sqrt{s}}\right), \quad (61)$$

where

$$\alpha = \sqrt{\mu_o \sigma y^2}. \quad (62)$$

Using the formula

$$\tilde{L}^{-1}\left(e^{-\alpha\sqrt{s}}\right) = \frac{\alpha}{2\sqrt{\pi t^3}} e^{-\alpha^2/4t} = \psi(y, t) \quad (63)$$

then yields

$$Q_n(\tau) = e^{-r_n \tau} \cdot \frac{\alpha}{2\sqrt{\pi t^3}} e^{-\frac{\alpha^2}{4\tau}} = e^{-r_n \tau} \psi(y, \tau) \quad : y > 0. \quad (64)$$

Equation (56) is simplified using the result

$$F_n(t) = F_{-n}(t) = \frac{-\mu_o \Omega_n}{2} \delta(t). \quad (65)$$

Substituting equations (64) and (65) into equation (56) yields

$$B_x(x, y, t) = \frac{-\mu_o}{2} \sum_{n=-\infty}^{n=+\infty} \Omega_n \int_0^t \delta(t-\tau) e^{-r_n \tau} \psi(y, \tau) e^{j\gamma_n x} d\tau. \quad (66)$$

Using the formulas

$$\Omega_{-n} = \Omega_n, \quad (67a)$$

$$r_{-n} = \frac{\gamma_n^2}{\mu_o \sigma} - j\nu \gamma_n = r_n^*, \quad (67b)$$

and

$$\gamma_{-n} = -\gamma_n = \frac{-2n\pi}{L}, \quad (67c)$$

reduces equation (66) to the simpler forms

$$B_x = -\mu_o \sum_{n=1}^{\infty} \Omega_n \int_0^t \delta(t-\tau) \psi(y, \tau) e^{\frac{\gamma_n^2 \tau}{\mu_o \sigma}} \cos(\gamma_n x - \gamma_n \nu \tau) d\tau \quad (68)$$

and

$$B_x = -\mu_o \sum_{n=1}^{\infty} \Omega_n \psi(y, t) e^{\frac{\gamma_n^2 t}{\mu_o \sigma}} \cos(\gamma_n x - \gamma_n \nu t) \quad (69)$$

We now compute $B_y(x, y, t)$ by taking the inverse Laplace transform of equation (48).

Using equations (50), (54a - c), and (58), we initially have

$$\begin{aligned}\tilde{B}_y &= \sum_{n=-\infty}^{n=+\infty} \tilde{P}_n(s) e^{-k_n y} e^{j\gamma_n x} \\ &= - \sum_{n=-\infty}^{n=+\infty} \frac{j\gamma_n}{\sqrt{\mu_o \sigma} \sqrt{s+r_n}} \left(\frac{\mu_o \Omega_n}{2} \right) e^{-\sqrt{\mu_o \sigma} \sqrt{s+r_n} y} e^{j\gamma_n x},\end{aligned}\quad (70)$$

followed by

$$B_y(x, y, t) = \frac{-j}{2} \sqrt{\frac{\mu_o}{\sigma}} \int_0^t \delta(t-\tau) \sum_{n=-\infty}^{n=+\infty} \gamma_n \Omega_n e^{j\gamma_n x} \Gamma_n(\tau) d\tau, \quad (71)$$

where

$$\Gamma_n(\tau) = \tilde{L}^{-1} \left(\frac{1}{\sqrt{s+r_n}} e^{-(\sqrt{\mu_o \sigma} \sqrt{s+r_n} y)} \right). \quad (72)$$

Using equation (61), we get

$$\begin{aligned}\Gamma_n(\tau) &= e^{-r_n \tau} \tilde{L}^{-1} \left(\frac{1}{\sqrt{s}} e^{-\alpha \sqrt{s}} \right) \\ &= e^{-r_n \tau} \frac{1}{\sqrt{\pi \tau}} e^{-\frac{\mu_o \sigma y^2}{4\tau}} = e^{-r_n \tau} \Phi(y, \tau),\end{aligned}\quad (73)$$

where

$$\Phi(y, \tau) = \frac{1}{\sqrt{\pi \tau}} e^{-\frac{\mu_o \sigma y^2}{4\tau}}. \quad (74)$$

Substituting equations (47), (73), and (74) into equation (71) and then integrating over τ gives

$$B_y = \frac{-j}{2} \sqrt{\frac{\mu_o}{\sigma}} \frac{1}{\sqrt{\pi t}} e^{-\frac{\mu_o \sigma y^2}{4t}} \sum_{n=-\infty}^{n=+\infty} e^{-\frac{\gamma_n^2 t}{\mu_o \sigma}} \gamma_n \Omega_n e^{j\gamma_n x} e^{-j\gamma_n vt} \quad (75)$$

Since γ_n is an odd function of n , while Ω_n is an even function of n , we get

$$\gamma_{-n} \Omega_{-n} = -\gamma_n \Omega_n. \quad (76)$$

Combining positive and negative values of n , and using equation (76) gives

$$\gamma_n \Omega_n e^{j\gamma_n(x-vt)} + \gamma_{-n} \Omega_{-n} e^{+j\gamma_{-n}(x-vt)} = 2 j\gamma_n \Omega_n \sin(\gamma_n x - \gamma_n vt). \quad (77)$$

Inserting equation (77) into equation (75) yields the following expression for B_y :

$$B_y = \sqrt{\frac{\mu_o}{\sigma}} \frac{1}{\sqrt{\pi t}} e^{-\frac{\mu_o \sigma y^2}{4t}} \sum_{n=1}^{n=+\infty} e^{-\frac{\gamma_n^2 t}{\mu_o \sigma}} \gamma_n \Omega_n \sin(\gamma_n x - \gamma_n vt). \quad (78)$$

Lastly, the current density in the moving conductor is determined from the formula

$$\vec{j} = \nabla \times \vec{H} = \frac{1}{\mu_o} \nabla \times \vec{B}. \quad (79)$$

4. Characterization of External Magnetic Field

The purpose of this section is to calculate the environmental magnetic field in the region below the source conductors (see Figure 1), that is, for field points satisfying the condition $y_0 < -w$. The magnetic field at the point x_0, y_0, z_0 is determined in a straightforward way using the Biot-Savart formula of equation (1) with x, y, z replaced by x_0, y_0, z_0 . The volumetric integration in equation (1) is over all current densities.

In our problem, there are two current sources that contribute to the environmental magnetic field: the first is the source from the input current source elements and the second is from the spatial distribution of current density within the moving conductor.

Using the formula

$$\nabla \times \vec{B} = \vec{k} \left(\frac{\partial B_y}{\partial x} - \frac{\partial B_x}{\partial y} \right), \quad (80)$$

the z-component of current density in the moving conductor is given by

$$j_c = \frac{1}{\mu_o} \left(\frac{\partial B_y}{\partial x} - \frac{\partial B_x}{\partial y} \right). \quad (81)$$

The z-component is the only component of current density in our system and is a consequence of the geometry. Using the results of section 3, which provide B_x and B_y as a function of x, y , and t , we can calculate the spatial distribution of current density for the moving conductor. When the resulting expression for j_c is inserted in equation (1), the environmental magnetic field from the moving conductor is determined as a function of x_0, y_0, z_0 , and in the region $y_0 < -w$.

In contrast to the exact computation of the environmental field from the spatial distribution of current density within the moving conductor, the contribution from the source current is relatively easy. The y -dimension of the source current is assumed to be very thin compared with $|y_0 - w|$. For the moving conductor, the vertical integrated current (i.e., image) is

$$J^* = \int_0^{\infty} j_c(y) dy = \frac{1}{\mu_0} \left[\frac{\partial}{\partial x} \int_0^{\infty} B_y(x, y, t) dy - \int_0^{\infty} \frac{\partial B_x(x, y, t)}{\partial y} dy \right]. \quad (82)$$

Placing J^* at some equivalent height above the ground plane $y = 0$ is analogous to placing an image current a distance $w_c = w + d$ above a finite conducting ground plane.

From the infinite conductivity case, we know that the current in the conductor will act to compensate the magnetic field generated by the source current. For this $\sigma = \infty$ case, the integrated vertical current is a continuous planar distribution, 180° out of phase with the source current. This image is located a distance w above the $y = 0$ plane. The resultant environmental field will be the smallest in this case because it is composed of two parts that nearly cancel each other when $|y_0| < -w$.

When $\sigma \neq \infty$, the image current cannot be placed any closer to $y = 0$ than w . This is true irrespective of the velocity. In the other extreme, we can place the image current so far above the $y = 0$ plane (this is only a mathematical abstraction) that the environmental magnetic field will be due to only the source current elements.

In summary, the upper bound on the environmental magnetic field will be determined by completely neglecting the current in the moving conductor. The lower bound will be computed by locating the image current a distance w above the $y = 0$ plane. We choose to render the results in this format, not because we cannot calculate the distant magnetic fields exactly [j_c can be calculated exactly from equation (81) for use in the Biot-Savart

law], but because this viewpoint provides enhanced insight into the salient physical processes.

Equation (82) can be formally integrated to yield

$$J^* = \frac{1}{\mu_o} [G(x,t) - B_x(x, y = \infty, t) + B_x(x, y = 0, t)], \quad (83)$$

where

$$G(x,t) = \int_0^\infty \frac{\partial B_y(x, y, t)}{\partial x} dy. \quad (84)$$

Taking the partial of equation (78) with respect to x and then integrating over y gives

$$G(x,t) = \frac{1}{\sigma} \sum_{n=1}^{n \rightarrow \infty} e^{-\frac{\gamma_n^2 t}{\mu_o \sigma}} \gamma_n^2 \Omega_n \cos(\gamma_n x - \gamma_n vt). \quad (85)$$

The exponential terms in equation (85) are a result of **diffusion** in the x -direction. The modal diffusion time constants are given by

$$t_{dn} = \frac{\mu_o \sigma}{\gamma_n^2} = \frac{\mu_o \sigma L^2}{4n^2 \pi^2}. \quad (86)$$

Using $\mu_o = 4\pi \times 10^{-7} \text{ H/m}$, $\sigma = 2.2 \times 10^7 \text{ mhos/m}$, and a nominal dimension of $L = 0.5 \text{ m}$ gives

$$t_{d1} = 0.18 \text{ s} \quad (87)$$

for the first mode. Even though higher-order modes will have shorter diffusion times, they will generally be much longer than the pulse lengths of interest—typically in the millisecond range. We return to this time-constant issue after our general analysis is completed.

Returning to equation (83), we note that since $B_x(x, y = \infty, t) = 0$, we can use equations (34) and (35) to write

$$J^* = \frac{G(x, t) + B_x(x, y = 0, t)}{\mu_o} - \frac{G(x, t)}{\mu_o} \delta(t) \sum_{n=1}^{\infty} \Omega_n \cos \gamma_n x. \quad (88)$$

Because all the magnetic field components determined up to this point were based on the impulse function, so is J^* . Applying the integral relationship of equation (37) as applied to J^* , the step function response for the total current per unit length is

$$J_{step}^* = A_j \int_0^t J^*(t - \tau) d\tau = A_j \int_0^t J^*(\tau) d\tau. \quad (89)$$

When equation (88) is inserted into equation (89), we get two contributions, which are distinctly associated with the image contribution described in section 2 and another part that is identified with diffusion and motion. We write

$$J_{step}^* = J_{DM}^* - J_I^*, \quad (90)$$

where the image contribution is given by

$$J_I^* = A_j \int_0^t \delta(\tau) d\tau \sum_{n=1}^{\infty} \Omega_n \cos \gamma_n x = A_j \sum_{n=1}^{\infty} \Omega_n \cos \gamma_n x, \quad (91)$$

and the diffusion-motion contribution is given by

$$J_{DM}^* = \frac{A_J}{\mu_o} \int_0^t G(x, \tau) d\tau. \quad (92)$$

Equation (92) is evaluated using equation (85). Before presenting the general result, it is instructive to evaluate J_{DM}^* for the special case of a stationary conductor, $v = 0$. These results **confirm** the assertions rendered in section 2. When $v = 0$, we have

$$G(x, t) = \frac{1}{\sigma} \sum_{n=1}^{n=\infty} e^{-\frac{\gamma_n^2 t}{\mu_o \sigma}} \gamma_n^2 \Omega_n \cos \gamma_n x, \quad (93)$$

and

$$J_{DM}^* = \frac{A_J}{\mu_o} \int_0^t G(x, \tau) d\tau = A_J \sum_{n=1}^{n=\infty} \Omega_n (1 - e^{-\frac{t}{t_{dn}}}) \cos \gamma_n x. \quad (94)$$

In carrying out the integration in equation (94), we have used the formula

$$\int_0^t e^{-\frac{\gamma_n^2 \tau}{\mu_o \sigma}} d\tau = \frac{\mu_o \sigma}{\gamma_n^2} (1 - e^{-\frac{\gamma_n^2 t}{\mu_o \sigma}}). \quad (95)$$

Equations (91) and (94) are rich in physical content and can be traced back to the discussion of section 2. If we let $\sigma = \infty$, then $t_{dn} = \infty$, all the “()” terms of equation (94) vanish, and we are left with only the image contribution,

$$J_{step}^* = -J_I^*. \quad (96)$$

By comparing equation (94) with equation (91) on a term-by-term basis and noting that

$$(1 - e^{-\frac{t}{t_{dn}}}) \leq 1, \quad (97)$$

we readily show that, on the average, over the periodic spatial interval $\{0, L\}$, the magnitude of J_{DM}^* is less than the magnitude J_I^* . The proof is straightforward using the orthogonality of the cosine terms. We have

$$|J_{DM}^*|_{ave} = \left(\frac{1}{L} \int_0^L (J_{DM}^*)^2 dx \right)^{1/2} = \left(\frac{A_J^2}{2} \sum_{n=1}^{\infty} \Omega_n^2 (1 - e^{-t/t_{dn}})^2 \right)^{1/2}, \quad (98)$$

and

$$|J_I^*|_{ave} = \left(\frac{1}{L} \int_0^L (J_I^*)^2 dx \right)^{1/2} = \left(\frac{A_J^2}{2} \sum_{n=1}^{\infty} \Omega_n^2 \right)^{1/2}. \quad (99)$$

For all real physical systems, $|J_I^*|_{ave}$ must be bounded and, hence,

$$\left(\frac{A_J^2}{2} \sum_{n=1}^{\infty} \Omega_n^2 \right)^{1/2} < \infty. \quad (100)$$

Every term in the series of equations (98) and (99) is positive. Since each term in equation (99) is greater than the corresponding term in equation (98), the proof that $|J_I^*|_{ave} > |J_{DM}^*|_{ave}$ is complete. In the regime where $t \ll t_{dn}$, we have the approximation

$$1 - e^{-t/t_{dn}} \approx t/t_{dn} \ll 1. \quad (101)$$

In this case, image theory provides a very good description of current flow.

Lastly, we notice that equations (91) and (94) can be inserted in equation (90) to give the result for a stationary conductor based on a first-order perturbation to the perfect conductor solution at $y = 0$

$$J_{step}^* = -A_J \sum_{n=1}^{m=\infty} \Omega_n e^{-\frac{t}{\tau_n}} \cos \gamma_n x. \quad (102)$$

Equation (102) shows that the current in the conductor will eventually vanish for a step function excitation and is due to conductive energy loss.

We now consider the general case involving a moving conductor, which requires use of equation (85) in equation (92). This calculation is facilitated by first writing

$$\cos(\gamma_n x - \gamma_n vt) = \cos(\gamma_n x) \cos(\gamma_n vt) + \sin(\gamma_n x) \sin(\gamma_n vt). \quad (103)$$

Inserting equation (103) into equation (85) gives

$$G(x, t) = G_1(x, t) + G_2(x, t), \quad (104)$$

where

$$G_1(x, t) = \frac{1}{\sigma} \sum_{n=1}^{n=\infty} e^{-\frac{\gamma_n^2 t}{\mu_0 \sigma}} \gamma_n^2 \Omega_n \cos(\gamma_n x) \cos(\gamma_n vt) \quad (105)$$

and

$$G_2(x, t) = \frac{1}{\sigma} \sum_{n=1}^{n=\infty} e^{-\frac{\gamma_n^2 t}{\mu_0 \sigma}} \gamma_n^2 \Omega_n \sin(\gamma_n x) \sin(\gamma_n vt). \quad (106)$$

Substituting equations (104) – (106) into equation (92) and integrating yields

$$J_{DM}^* = \frac{A_J}{\mu_o \sigma} \sum_{n=1}^{n=\infty} \gamma_n^2 \Omega_n \cos(\gamma_n x) \Psi_{nc}(t) + \frac{A_J}{\mu_o \sigma} \sum_{n=1}^{n=\infty} \gamma_n^2 \Omega_n \sin(\gamma_n x) \Psi_{ns}(t), \quad (107)$$

where

$$\Psi_{nc} = \frac{1}{\left((\gamma_n^2 / \mu_o \sigma)^2 + (\gamma_n v)^2 \right)} \left(\frac{\gamma_n^2}{\mu_o \sigma} - e^{-\frac{\gamma_n^2 t}{\mu_o \sigma}} \left(\frac{\gamma_n^2}{\mu_o \sigma} \cos(\gamma_n vt) - \gamma_n v \sin(\gamma_n vt) \right) \right) \quad (108)$$

and

$$\Psi_{ns} = \frac{1}{\left((\gamma_n^2 / \mu_o \sigma)^2 + (\gamma_n v)^2 \right)} \left(\gamma_n v - e^{-\frac{\gamma_n^2 t}{\mu_o \sigma}} \left(\frac{\gamma_n^2}{\mu_o \sigma} \sin(\gamma_n vt) + \gamma_n v \cos(\gamma_n vt) \right) \right). \quad (109)$$

The foregoing expressions show that the conductor current contains harmonics with angular frequencies:

$$\omega_n = \gamma_n v = \frac{2n\pi v}{L}. \quad (110)$$

Using values of $L = 0.5 \text{ m}$, and $v = 200 \text{ m/s}$ gives

$$\omega_1 = 2,500 \text{ rad/s} \quad (111)$$

for the first harmonic.

The damping time constants given by equation (86) show that the higher harmonics dampen out much more rapidly than the lower numbered ones. This damping produces frequency broadening, which must be taken into account when analyzing the response of electronic equipment that is located near the system of conductors shown in Figure 1.

In order to better understand the essential features of environmental magnetic fields generated by the moving conductor current system of Figure 1, it is desirable to compare the magnitude of the modal terms in equation (107) with the corresponding modal terms of J_I^* as given by equation (91). We shall use the same procedure for making this comparison as we did in the development of equations (98) and (99).

Using the orthogonality of both cosine and sine function in computing $|J_{DM}^*|_{ave}$ from equation (107), we obtain

$$|J_{DM}^*|_{ave} = \left(\frac{A_J^2}{2} \sum_{n=1}^{n=\infty} H_n^2 \Omega_n^2 \right)^{1/2}, \quad (112)$$

where

$$H_n^2 = \frac{\Psi_{nc}^2}{t_{dn}^2} + \frac{\Psi_{ns}^2}{t_{dn}^2}. \quad (113)$$

With the help of basic trigonometry, algebra, and equations (108) and (109), we readily prove that

$$H_n^2 = \frac{n^2}{n^2 + (t_{d1}\omega_1)^2} h_n(t), \quad (114)$$

where

$$h_n(t) = 1 + e^{-\frac{2t}{t_{dn}}} - 2e^{-\frac{t}{t_{dn}}} \cos \omega_n t. \quad (115)$$

Figures 5 and 6 show $h_n(t)$ and $H_n^2(t)$, respectively, as a function of time with mode number, n , as a parameter for $\mu_o = 4\pi \times 10^{-7} \text{ H/m}$, $\sigma = 2.2 \times 10^7 \text{ mhos/m}$, $L = 0.5 \text{ m}$, and $v = 200 \text{ m/s}$.

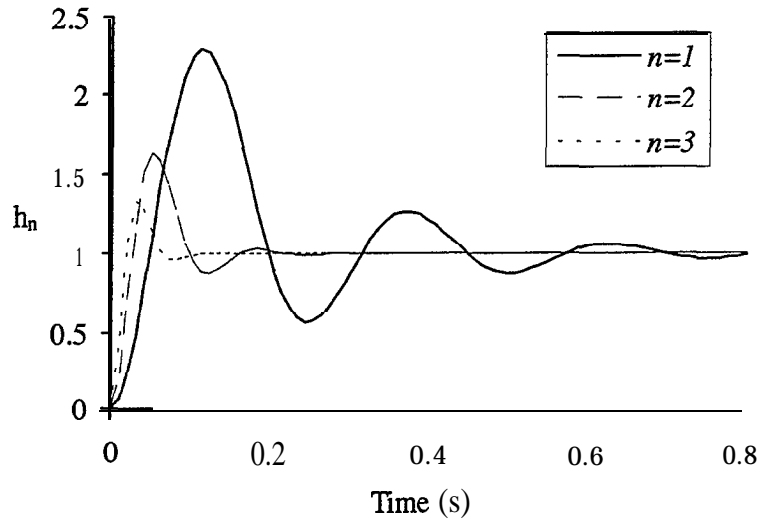


Figure 5. $h_n(t)$ as a Function of Time With Mode Index, n , as Parameter.

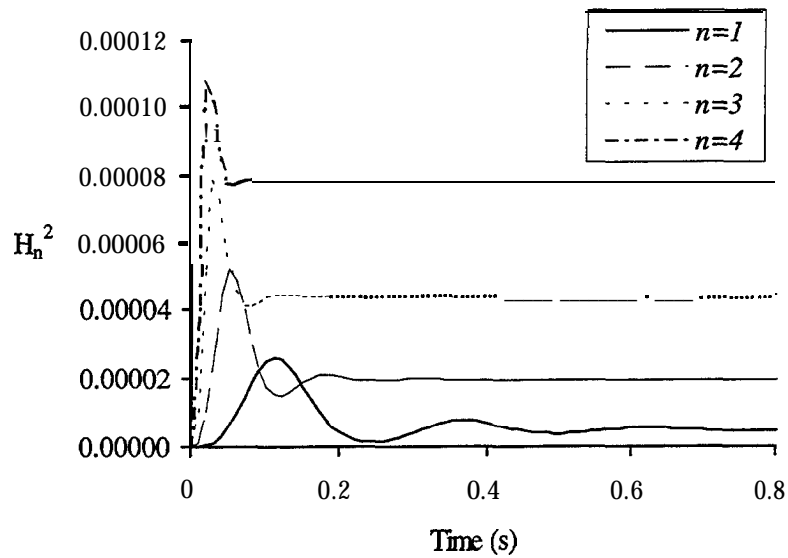


Figure 6. $H_n^2(t)$ as a Function of Time With Mode Index, n , as Parameter.

By comparing equation (112) with equation (99) on a term-by-term basis, we note that their ratios are \mathbf{H}_n^2 . Equation (115) shows that the maximum value of $h_n(t)$ is four. Thus, for this exploratory study, with the mode index, n , less than 10, \mathbf{H}_n^2 can be approximated by its upper bound as

$$\mathbf{H}_n^2 \approx \frac{4n^2}{n^2 + (t_{d1}\omega_1)^2}. \quad (116)$$

We also have

$$t_{d1}\omega_1 = 0.18 (2,500) = 450. \quad (117)$$

The higher order terms of $|J_{DM}^*|_{ave}$ become comparable to those of $|J_I^*|_{ave}$ when \mathbf{H}_n^2 approaches unity. Equations (116) and (117) show that this will occur when the mode index becomes greater than

$$n^* = \left(\frac{t_{d1}\omega_1}{3} \right)^{1/2} = 260. \quad (118)$$

Considering the first few modes, $|J_{DM}^*|_{ave}$ will be significantly less than $|J_I^*|_{ave}$. The motion of the conductor does not appreciatively affect the environmental field.

For the purposes of calculating and bounding the environmental magnetic field in the region $y_0 < -w$ we need to consider the real current density source located in the plane $y = -w$ and its image current density source located in the plane $y = +w$ (see Figures 1 and 2). As previously mentioned, the maximum environmental magnetic field will occur when the image contribution is absent and the smallest will occur when the image is

included. These two limits bound the problem, irrespective of how well we calculate the details of the current in the moving conductor.

The starting point for the calculation of the magnetic field at position

$$\vec{r}_o = \vec{i}x_o + \vec{j}y_o + \vec{k}z_o \quad (119)$$

is the Biot-Savart law, which is given by equation (1). In order to be consistent with the notation of section 3, we let x, y, z be the coordinates of the volumetric distribution of current density; the reader may recall that, in section 2, $\bar{x}, \bar{y}, \bar{z}$ were used for the volumetric distribution of current density. When we consider only the real source and its image, the magnetic field at \vec{r}_o is given by

$$\vec{B}(\vec{r}_o) = \vec{B}_R(\vec{r}_o) + \vec{B}_I(\vec{r}_o), \quad (120)$$

where \vec{B}_R and \vec{B}_I are the contributions from the real and image sources, respectively.

They are given by

$$\vec{B}_R = \frac{\mu_o}{4\pi} \int_{-\infty}^{+\infty} \int_{-h}^{+h} \frac{\vec{k}dz \times \vec{r}_R}{|\vec{r}_R|^3} J_R(x) dx \quad (121)$$

and

$$\vec{B}_I = -\frac{\mu_o}{4\pi} \int_{-\infty}^{+\infty} \int_{-h}^{+h} \frac{\vec{k}dz \times \vec{r}_I}{|\vec{r}_I|^3} J_R(x) dx, \quad (122)$$

where the integration over x extends from $-\infty$ to $+\infty$, the integration over z extends from $-h$ to $+h$:

$$\vec{r}_R = \vec{i}(x_o - x) + \vec{j}(y_o + w) + \vec{k}(z_o - z), \quad (123a)$$

$$\vec{k} \times \vec{r}_R = \vec{j}(x_o - x) - \vec{i}(y_o + w), \quad (123b)$$

$$|\vec{r}_R|^3 = \left((x_o - x)^2 + (y_o + w)^2 + (z_o - z)^2 \right)^{3/2}, \quad (123c)$$

$$\vec{r}_I = \vec{i}(x_o - x) + \vec{j}(y_o - w) + \vec{k}(z_o - z), \quad (123d)$$

$$\vec{k} \times \vec{r}_I = \vec{j}(x_o - x) - \vec{i}(y_o - w), \quad (123e)$$

and

$$|\vec{r}_I|^3 = \left((x_o - x)^2 + (y_o - w)^2 + (z_o - z)^2 \right)^{3/2}. \quad (123f)$$

In equations (123a - f), we place no restriction on the location of the field point, although we apply the results to those locations where $y_o < -w$.

The negative sign in equation (122) and the appearance of J_R **in the** integral accounts for the fact that the image current is the negative of the real current. Equations (123a - f) account for the fact (see Figure 2) that the source current density is located at $y = -w$, while the image current density is located at $y = +w$. J_R is determined from equations (21) and (24), with J_o given by the step function of equation (38). We have

$$J_R(x) = \sum_{n=1}^{\infty} A_n \cos \frac{2n\pi x}{L} \quad (124)$$

and

$$A_n = \frac{2A_J}{n\pi} (1 - \cos n\pi) \sin \frac{n\pi l_1}{L}. \quad (125)$$

The calculation of the analytical forms for \vec{B}_R and \vec{B}_I is straightforward. For brevity, we calculate \vec{B}_R and then simply determine \vec{B}_I by substituting $y_o - w$ in place of $y_o + w$ and taking the negative of the result. Equation (121) is first integrated over z to yield

$$\vec{\Gamma} = \int_{-h}^{+h} \frac{\vec{k} dz \times \vec{r}_R}{|\vec{r}_R|^3} = -\vec{i}(y_o + w)W + \vec{j}(x_o - x)W, \quad (126)$$

where

$$W = \int_{-h}^{+h} \frac{dz}{(b^2 + (z_o - z)^2)^{3/2}}, \quad (127)$$

and

$$b^2 = (x_o - x)^2 + (y_o + w)^2. \quad (128)$$

The integration in equation (126) gives

$$W = \frac{1}{b^2} \left[\frac{z_o + h}{((z_o + h)^2 + b^2)^{1/2}} - \frac{z_o - h}{((z_o - h)^2 + b^2)^{1/2}} \right]. \quad (129)$$

The foregoing expression simplifies when we take our observation point to be located at the midpoint, $z_o = 0$. There is **essentially** no loss of generality in this case, and W becomes

$$W = \frac{2}{b^2} \left[\frac{h}{(h^2 + b^2)^{1/2}} \right]. \quad (130)$$

Since one of the principle aims of this study is to examine the relationship between the distance of the field point from the conductors as compared to the spatial periodicity of the current in the moving conductor, we further simplify W by setting $x_o = 0$. Equation (130) then reduces to

$$W = \frac{2h}{x^2 + (y_o + w)^2} \frac{1}{(h^2 + x^2 + (y_o + w)^2)^{1/2}}. \quad (131)$$

Equation (131) is used in subsequent calculations.

The procedure from this point is to substitute equations (124), (126), and (131) into equation (121) and then integrate over x between the limits of $-\infty$ to $+\infty$. Formally integrating over x initially yields

$$\bar{B}_R = -\frac{\mu_o}{4\pi} \left[\bar{i}(y_o + w) \int_{-\infty}^{+\infty} J_R W dx + \bar{j} \int_{-\infty}^{+\infty} J_R x W dx \right]. \quad (132)$$

Since J_R and W are symmetric functions of x , and the “ x ” in the second integral is an antisymmetric function of x , the second integral vanishes. Inserting equations (124) and (131) into equation (132) gives

$$\bar{B}_R = -\frac{\mu_o}{4\pi} \left[\bar{i}(y_o + w) \sum_{n=1}^{n=\infty} A_n \Theta_n(y_o + w, h) \right], \quad (133)$$

where

$$\Theta_n = \int_{-\infty}^{+\infty} \cos \frac{2n\pi x}{L} \frac{2h}{x^2 + (y_o + w)^2} \frac{1}{(h^2 + x^2 + (y_o + w)^2)^{1/2}} dx. \quad (134)$$

Simplification results when we cast the foregoing equations in dimensionless form by introducing the variables

$$\rho = \frac{x}{L}, \quad (135)$$

$$\eta = \frac{y_o + w}{L}, \quad (134)$$

and selecting a specific value for h . For convenience a value of $h = L$ is used.

Using equations (125), (135), and (136) we derive the following expression for B_R , recalling from equation (133) that it is the x-component (hence we drop the vector notation):

$$B_R = -\frac{\mu_o}{4\pi} A_j \sum_{n=1}^{n=\infty} a_n P_n(\eta), \quad (137)$$

where

$$a_n = \frac{2}{n\pi} (1 - \cos n\pi) \sin \frac{n\pi l_1}{L} \quad (138)$$

and

$$P_n = 4\eta \int_0^{\infty} \frac{\cos 2n\pi \rho}{(\eta^2 + \rho^2)(1 + \eta^2 + \rho^2)^{1/2}} d\rho. \quad (139)$$

Figure 7 shows P_n as a function of positive η , with mode index, n , as parameter. As expected, P_n decreases with increasing distance from the moving conductor and with increasing mode index. We also have

$$P_n(-\eta) = -P_n(\eta), \quad (140)$$

which is relevant in our calculations since y_o is negative.

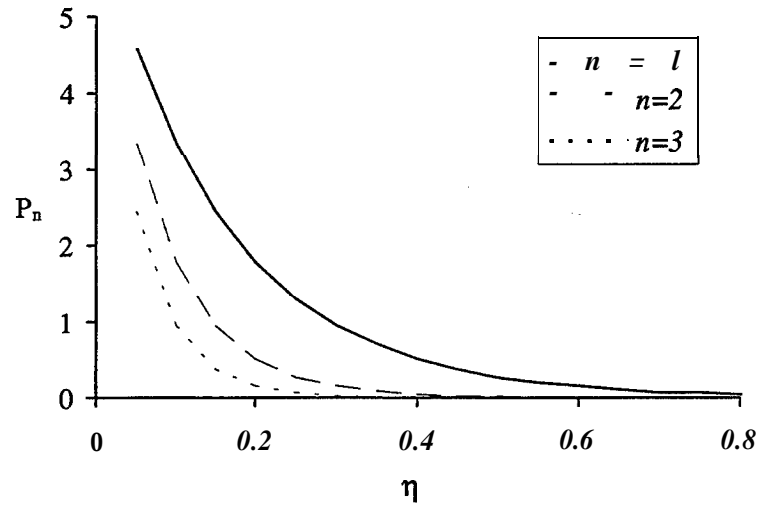


Figure 7. $P_n(\eta)$ as a Function of Positive η With Mode Index as Parameter.

The total magnetic field is computed from the formalism of equations (120) to (123). In terms of the field point used in the foregoing calculations $x_o = 0, z_o = 0$, we have

$$B_{net} = B_R(\eta) - B_R\left(\eta - \frac{2w}{L}\right), \quad (141)$$

the second term being attributed to the image.

5. Numerical Results

The purpose of this section is to obtain numerical estimates of the magnetic flux density as a function of vertical distance from the source conductor system for a particular set of parameters. The following values are used:

$$l_1 = 17.5 \text{ mm},$$

$$l_2 = 7.5 \text{ mm},$$

$$L = 2(l_1 + l_2) = 0.5 \text{ m},$$

$$w = 2.5 \text{ mm},$$

$$h = L,$$

and

$$I_o = 600,000 \text{ A}.$$

There is a wide range of magnetic field variations in this system. The highest fields occur very close to the source elements themselves. In this region, which is not anticipated to be close to any external electronics systems in practical applications, the magnetic field intensity is of the order of

$$\mathbf{H} \approx \frac{I_o}{l_1} = \mathbf{A} = 3.4 \text{ kA/mm} \quad (142)$$

and the magnetic flux density is

$$\mathbf{B} = \mu_o \mathbf{H} = 4.2 \text{ T.} \quad (143)$$

As we move away from the individual conductors, the influence of the periodic array of the source current is seen and the theory provided in the previous section must be used. The largest fields in this case exist when the image effect is negligible. This occurs when the image distance becomes large. As previously discussed, the case in which the image currents can be neglected is a mathematical abstraction and provides a limiting case of maximum environmental magnetic field. This field is given by

$$B_{net} = B_R = -\frac{\mu_o}{4\pi} A_J \sum_{n=1}^{n=\infty} a_n P_n(\eta). \quad (144)$$

Using the numbers provided at the beginning of this section and noting from equation (138) that

$$a_n = 0 \quad : n = \text{even number,} \quad (145)$$

we obtain $a_1 = 1.15$ and $a_3 = -0.064$.

Subsequent values of a_n are negligible. Moreover, when a_1 and a_3 are combined with the results of Figure 7, we see that the third harmonic is just a few percent of the first harmonic. Hence, with very good approximation, we can use the result

$$B_R \cong +\frac{\mu_o}{4\pi} A_J a_1 P_1(-\hat{\eta}), \quad (146)$$

where the dimensionless distance is

$$\hat{\eta} = \frac{-|y_o| + w}{L} = -\frac{(|y_o| - w)}{L}. \quad (147)$$

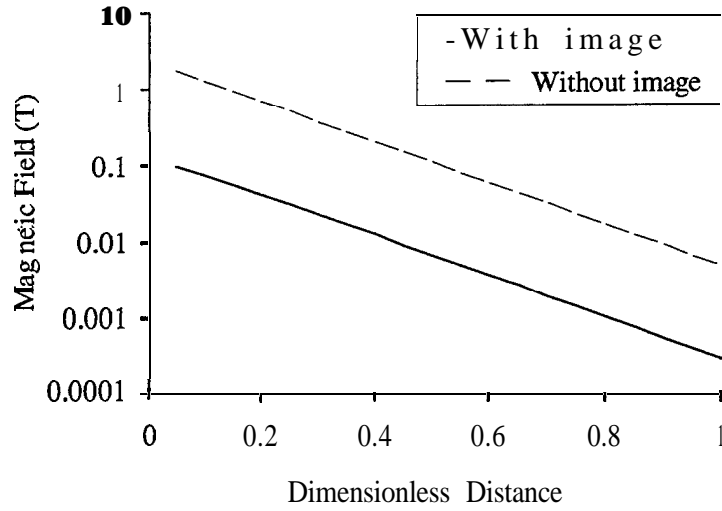


Figure 8. Magnetic Field as a Function of Dimensionless Distance.

In the foregoing equation, we have adjusted for the fact that y_o is negative. Figure 8 is a plot of B_R (without the image current) as a function of $\hat{\eta}$.

When the image is taken into account, we must use equation (141), which now becomes

$$B_{net} = B_R(-\hat{\eta}) - B_R(-\hat{\eta} - \frac{2w}{L}). \quad (148)$$

A plot of equation (148) is also shown in Figure 8. As observed, the magnetic field with the contribution from the image current reduces the environmental field by more than an order of magnitude. However, in both cases, the field has decayed roughly 3 orders of magnitude at one conductor spacing (L) from the source.

6. Summary and Conclusions

We have developed a model for determining the space-and-time behavior of the magnetic field external to a system of moving pulsed conductors. The model includes a moving finite conductivity conductor in relative close proximity to a stationary conductor. The analysis indicates that the magnetic field has a space-and-time **periodicity** that can be related to the parameters of the conductors. Furthermore, we present a numerical example that predicts the magnitude and frequency of the magnetic field as a function of distance from the stationary conductor. In this analysis we show that the induced currents are nearly equal in magnitude to those in the source. The eddy currents in the moving conductor delay the penetration of the magnetic flux. The environmental magnetic field decays rapidly to negligible levels at distances of interest to the EMC problem.

One of the more interesting and potentially important devices currently in development is the air-core pulsed alternator. These devices have been used to deliver large currents for electromagnetic launch systems. The main difference between a conventional generator and a pulsed alternator is the latter's extensive use of compensation. Compensation is a method of reducing the inductance associated with an alternator's armature winding. This reduction is achieved by inducing currents in a moving conductor that is in close proximity to the armature winding of the alternator.

In order to estimate the environmental magnetic field produced by a moving pulsed conductor, we have assumed a step function current for the current source elements. In an actual alternator system, these currents would be produced as a result of voltage generation due to a spatially varying direct current excitation field established in the air gap between the moving conductor and the armature windings. Of course, this additional source would contribute to the environmental magnetic field. This excitation source has not been considered in this analysis but can readily be computed using the techniques developed in this study.

INTENTIONALLY LEFT BLANK

7. References

1. Bennett J., T. Gora, P. Kemmey, and W. Kolkert. "Electromagnetic Braking of a Metallic Projectile in Flight." *IEEE Transactions on Magnetics*, vol. 21, no. 3, May 1985.
2. Doyle, M. R., D. Samuel, T. Conway, and R. Klimowski. "Electromagnetic Aircraft Launch Systems – EMALS." *IEEE Transactions on Magnetics*, vol. 31, no. 1, pp. 528 - 533, January 1995.
3. Summerfield, M. "Development of a Linear Piston-Type Pulse Power Electric Generator for Powering Electric Guns." *IEEE Transactions on Magnetics*, vol. 29, no. 1, January 1993.
4. Kilgore, L. A., E. Hill, and C. Flick. "A New Three Million KVA Short Circuit Generator." *IEEE Transactions (Power Apparatus and Systems)*, no. 67, pp. 442 - 445, August 1963.
5. Pratap, S. and M. Driga. "Compensation in Pulsed Alternators." *IEEE Transactions on Magnetics*, vol 35, no. 1, pp. 372 - 377, January 1999.
6. Kohlberg, I., C. Le, and A. Zielinski. "Predictions and Observations of Transient Electric and Magnetic Fields Generated by Electromagnetic Launch Systems." Conference Paper, XXVII International Union of Radio Science (URSI) General Assembly, Lille, France, 28 August - 5 September 1996.
7. Zielinski, A. E., C. Le, J. Bennett, and I. Kohlberg. "Railgun Electric Fields: Experiment and Theory." *IEEE Transactions on Magnetics*, vol. 31, no. 1, pp. 463, January 1999.
8. Zielinski, A. E. "In-bore Magnetic Field Management." ARL-TR-1914, U.S. Army Research Laboratory, Aberdeen Proving Ground, MD, March, 1999.
9. Jordan, E. C. and K. G. Balmain. *Electromagnetic Waves and Radiating Systems*. 2nd Edition, Prentice-Hall, Inc. Englewood Cliffs, NJ, 1968.
10. Banos, A. *Dipole Radiation in the Presence of a Conducting Half-Space*. Pergamon Press, NY, 1966.
11. Hill, D. A., and J. R. Wait. "Diffusion of Electromagnetic Pulses Into the Earth From a Line Source." *IEEE Transactions on Antennas and Propagation*, vol. 1, pp. 145, January 1974.

12. Bannister, P. R. "The Image Theory Electromagnetic Fields of a Horizontal Dipole in the Presence of a Conducting Half Space." *Radio Science*, vol. 17, no. 5, pp. 1095, September - October 1982.

<u>NO. OF</u> <u>COPIES</u>	<u>ORGANIZATION</u>
2	DEFENSE TECHNICAL INFORMATION CENTER DTIC DDA 8725 JOHN J KINGMAN RD STE 0944 FT BELVOIR VA 22060-6218
1	HQDA DAMO FDQ DENNIS SCHMIDT 400 ARMY PENTAGON WASHINGTON DC 203 10-0460
1	OSD OUSD(A&T)/ODDDR&E(R) RJTREW THE PENTAGON WASHINGTON DC 20301-7100
1	DPTY CG FOR RDE us ARMY MATERIEL CMD AMCRD MG CALDWELL 5001 EISENHOWER AVE ALEXANDRIA VA 22333-0001
1	INST FOR ADVNCD TCHNLGY THE UNTV OF TEXAS AT AUSTIN PO BOX 20797 AUSTIN TX 78720-2797
1	DARPA B KASPAR 3701 N FAIRFAX DR ARLINGTON VA 22203-1714
1	NAVAL SURFACE WARFARE CTR CODE B07 J PENNELLA 17320 DAHLGREN RD BLDG 1470 RM 1101 DAHLGREN VA 22448-5100
1	US MILITARY ACADEMY MATH SCI CTR OF EXCELLENCE DEPT OF MATHEMATICAL SCI MAJ M D PHILLIPS THAYERHALL WEST POINT NY 10996-1786

<u>NO. OF</u> <u>COPIES</u>	<u>ORGANIZATION</u>
1	DIRECTOR US ARMY RESEARCH LAB AMSRL D RWWHALIN 2800 POWDER MILL RD ADELPHI MD 20783-1 145
1	DIRECTOR US ARMY RESEARCHLAB AMSRL DD J J ROCCHIO 2800 POWDER MILL RD ADELPHI MD 20783-1 145
1	DIRECTOR US ARMY RESEARCH LAB AMSRL CS AS (RECORDS MGMT) 2800 POWDER MILL RD ADELPHI MD 20783-1 145
3	DIRECTOR US ARMY RESEARCH LAB AMSRL CI LL 2800 POWDER MILL RD ADELPHI MD 20783-1145
	<u>ABERDEEN PROVING GROUND</u>
4	DIR USARL AMSRL CI LP (305)

<u>NO. OF COPIES</u>	<u>ORGANIZATION</u>
1	DIR FOR THE DIRECTORATE OF FORCE DEVELOPMENT US ARMY ARMOR CENTER COL E BRYLA FT KNOX KY 40121-5000
1	US ARMY MATERIAL COMMAND AMCDCG-T C KITCHENS 5001 EISENHOWER BLVD ALEXANDRTA VA 22333-0001
2	US ARMY RESEARCH LAB AMSRL SE RE CLE 2800 POWDER MILL RD ADELPHI MD 20783-1145
2	US ARMY RESEARCH LAB AMSTA AR CCF A G MCNALLY 2800 POWDER MILL RD ADELPHI MD 20783-1 145
1	DPTY ASST SEC FOR RD&A R CHAIT THE PENTAGON RM 3E480 WASHINGTON DC 20310-0103
1	OFC OF THE DIRECTOR DEFENSE RESEARCH AND ENGINEERING C KITCHENS 3080 DEFENSE PENTAGON WASHINGTON DC 20301-3080
1	us ARMY MISSILE COMMAND AMSMI RD DR MCCORKLE REDSTONE ARSENAL AL 35898-5240
2	US ARMY TACOM TARDEC JCHAPIN M TURNER AMSTA TR D MS #207 WARREN MI 48397-5000

<u>NO. OF COPIES</u>	<u>ORGANIZATION</u>
1	US ARMY TACOM-ARDEC J BENNETT FSAE-GCSS-TMA / BLDG 354 PICATINNY ARSENAL NJ 07806-5000
2	INST FOR ADVANCED TECH UNIV OF TEXAS AT AUSTIN P SULLIVAN F STEPHANJ 4030-2 WEST BRAKER LANE AUSTIN TX 78759-5329
3	UNIV OF TEXAS AT AUSTIN CENTER FOR ELECT A WALLS J KITZMILLER S PRATAP PRC MAIL CODE R7000 AUSTIN TX 78712
1	LOCKHEED-MARTIN-VOUGHT R TAYLOR PO BOX 650003 MS WT-21 DALLAS TX 75265-0003
1	INST FOR DEFENSE ANALYSIS I KOHLBERG 1801 N BEAUREGARD ST ALEXANDRIA VA 22311
1	UNIV AT BUFFALO SUNY/AB JSARJEANT PO BOX 601900 BUFFALO NY 14260-1900
2	UDLP B GOODELL R JOHNSON MS MI70 4800 EAST RIVER RD MINNEAPOLIS MN 55421-1498

**NO. OF
COPIES ORGANIZATION**

1 UNIV OF TEXAS AT AUSTIN
M DRIGA
ENS 434 DEPT OF ECE
MAIL CODE 60803
AUSTIN TX 78712

1 SAIC
G CHRYSSOMALLIS
3800 WEST 80TH ST
SUITE 1090
BLOOMINGTON MN
5543 1

1 SAIC
J BATTEH
1225 JOHNSON FERRY RD
SUITE 100
MARIETTA GA 30068

1 SAIC
K A JAMJSON
1247 B N EGLIN PKWY
SHALIMAR FL 32579

2 LAP RESEARCH INC
D BAUER
J BARBER
2763 CULVER AVE
DAYTON OH 45429-3723

3 MAXWELL TECHNOLOGIES
JKEZERIAN
P REIDY
T WOLFE
9244 BALBOA AVENUE
SAN DIEGO CA 92123

1 NORTH CAROLINA STATE UNIV
M BOURHAM
DEPT OF NUCLEAR ENGR
BOX 7909
RALEIGH NC 27695-7909

1 MAXWELL PHYSICS INTRNTNL
CGILMAN
2700 MERCED STREET
PO BOX 5010
SAN LEANDRO CA 94577-0599

**NO. OF
COPIES ORGANIZATION**

1 ATA ASSOCIATES
W ISBELL
PO BOX 6570
SANTA BARBARA CA 93 160-6570

1 PHILLIPS LABORATORY/WSR
C BAUM
KIRTLAND AFB NM 87117

1 CENTER FOR NAVAL ANALYSIS
F BOMSE
4401 FORD AVENUE
PO BOX 16268
ALEXANDRIA VA 22302-0268

1 SPECTRAL SYNTHESIS LABS
R GARDNER
6152 MANCHESTER PARK CIR
ALEXANDRIA VA 223 10-4957

ABERDEEN PROVING GROUND

23 DIR USARL
AMSRLWM
I MAY
L JOHNSON
AMSRL B
A HORST
E SCHMIDT
AMSRLWM TE J POWELL
AMSRLWMBE G WREN
AMSRL WM BD B FORCH
AMSRL WM BA W D'AMICO
AMSRLWM BC
P PLOSTINS
D LYON
JGARNER
v OSKAY
M BUNDY
J SAHU
PWEINACHT
H EDGE
B GUIDOS
A ZIELINSKI
DWEBB
K SOENCKSEN
S WILKERSON
T ERLINE
J NEWILL

INTENTIONALLY LEFT BLANK.

USER EVALUATION SHEET/CHANGE OF ADDRESS

This Laboratory undertakes a continuing effort to improve the quality of the reports it publishes. Your comments/answers to the items/questions below will aid us in our efforts.

1. **ARL** Report Number/Author ARL-TR-1931 (Kohlberg) Date of Report April 1999

2. Date Report Received _____

3. Does this report satisfy a need? (Comment on purpose, related project, or other area of interest for which the report will be used.) _____

4. Specifically, how is the report being used? (Information source, design data, procedure, source of ideas, etc.) _____

5. Has the information in this report led to any quantitative savings as far as man-hours or dollars saved, operating costs avoided, or efficiencies achieved, etc? If so, please elaborate. _____

6. General Comments. What do you think should be changed to improve future reports? (Indicate changes to organization, technical content, format, etc.) _____

**CURRENT
ADDRESS**

Organization

Name

E-mail Name

Street or P.O. Box No.

City, State, Zip Code

7. **If indicating** a Change of Address or Address Correction, please provide the Current or Correct address above and the Old or Incorrect address below.

**OLD
ADDRESS**

Organization

Name

Street or P.O. Box No.

City, State, Zip Code

(Remove this sheet, fold as indicated, tape closed, and mail.)
(DO NOT STAPLE)